Nuclear Instruments and Methods 198 (1982) 515–521
North-Holland Publishing Company

THE BRAGG LINESHAPES IN TIME-OF-FLIGHT NEUTRON POWDER SPECTROSCOPY

F. KROPFF, J.R. GRANADA and R.E. MAYER
*Centro Atómico Bariloche *, 8400 S.C. de Bariloche, Argentina*

Received 5 November 1981

A four-parameter function is proposed to describe the position, shape and integrated intensity of the Bragg peaks in a powder neutron time-of-flight diffraction spectrum. The wavelength dependence of the parameters is discussed in terms of geometry and time uncertainties. The proposed function and the variation of its parameters along the time scale are compared with experimental results.

1. Introduction

The use of pulsed neutron sources has proved to be a valuable tool in neutron diffraction studies of condensed matter. It has been pointed out that one of the more prominent features of an accelerator based pulsed source lies in its ability to produce a significant flux of epithermal neutrons, thus allowing powder diffraction measurements to be extended into the range of high values of the scattering vector ($Q \sim 25$ Å^{-1}), which in turn renders possible a greater accuracy in the determination of thermal and structural parameters.

The analysis of scattering spectra taken on powders using time of flight (TOF) techniques requires the knowledge of the shape of individual Bragg peaks. Their overlapping increases with Q, that is to say, at shorter times of flight. The base-line also increases with Q and has to be determined simultaneously with the coherent elastic spectrum. The ability to separate both components largely determines the upper Q limit which can be reached in the analysis and furthermore, the shape of the peaks in that region has to be extrapolated from the low Q region, where no overlap exists.

A precise description of the lineshapes is also relevant in the case where the powder spectrum is used for the calibration of the elastic Q scale in scattering experiments on liquid or amorphous materials.

It is well known that the peaks are asymmetrical, and several empirical models have been used by different authors to fit them:

a) two Gaussians joined at the top [1],

b) the convolution of a "triangular function" with the product of an exponential times a step function [2],

c) the convolution of a Gaussian with a two-exponentials composed function [3],

d) the joining of two Gaussians and an exponential tail [4].

The convolution-based models reflect the separation of the detection time "error" into a geometrical function and a source emission-time function. The drawback in those models was the large evaluation time required.

This work presents an alternative approach to the problem of peak shape description. The convolution method is employed using two different models to represent the emission-time distribution; the resulting integrals are solved in terms of analytical functions which require four parameters to describe the position, shape and integrated intensity of a Bragg peak. The dependence of these parameters on the neutron wavelength is illustrated through the analysis of scattering data taken on polycrystalline molybdenum.

2. Experimental

The scattering experiment was performed using a 25 MeV electron LINAC with a lead target as a pulsed neutron source.

The sandwich-type moderator was disk-shaped polypropylene, 152 mm in diameter and 25 mm thick with a 0.6 mm Cd sheet 6 mm beneath the viewed surface. The sample–source distance was 490 cm and the sample–detectors distance approximately 40 cm. The mean angle of the detectors was 161°.

Eight ^{3}He detectors (10 atm pressure, 1″ diameter, 6″ active length) were placed in pairs forming a square. Each symmetrical pair was placed in a configuration that simulated a surface of

$$tQ_{el} = \frac{4\pi m_n}{h} l \sin\theta = \text{constant}, \qquad (1)$$

where t is the neutron TOF, Q_{el} is the elastic scattering vector, m_n is the neutron mass, h is Planck's constant, l

* Comisión Nacional de Energia Atómica.

0167-5087/82/0000–0000/$02.75

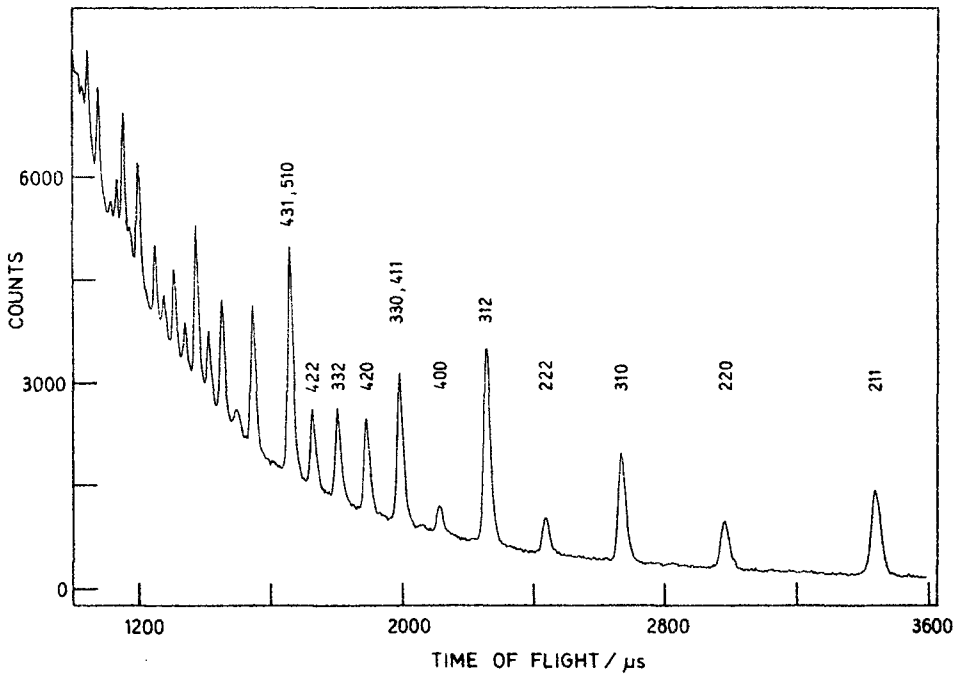

Fig. 1. The recorded time of flight scattering spectrum from polycrystalline molybdenum. For the sake of clarity, Miller indices for only some of the peaks are indicated.

is the total flight distance, and 2θ is the scattering angle. This is called a time focussed detector configuration [5].

Scattering data from polycrystalline molybdenum were collected during 72 h, with a LINAC repetition rate of 100 pulses per second. The observed TOF spectrum is shown in fig. 1.

3. The peak shape

The experience gained in neutron scattering using steady state neutron beams clearly indicates that geometry effects distort the Bragg lines into Gaussians [6]. To describe the source emission-time distribution in TOF experiments, we tried two different functions:

$$f_1'(t) = Y(t)\frac{1}{\alpha(\lambda)}\,e^{-t/\alpha(\lambda)}, \tag{2}$$

$$f_2'(t) = Y(t)\frac{1}{2a^3(\lambda)}\,t^2\,e^{-t/a(\lambda)}, \tag{3}$$

where $Y(t)$ is the step function.

Eq. (2) is suggested by the behaviour corresponding to the one-collission model, whereas eq. (3) is the asymptotic form (infinite energy source) of the time distribution for an infinite moderator in the slowing down energy region.

Provided the geometrical effects are negligible, the time distribution function should be reproduced at the detector with a delay equal to the time of flight t_0 for the wavelength considered. For example eq. (2) becomes

$$f_1(t) = Y(t-t_0)\frac{1}{\alpha(\lambda)}\,e^{-(t-t_0)/\alpha(\lambda)}. \tag{4}$$

The combined effect of geometry and emission time distributions is represented by the convolution of eq. (4) with the Gaussian

$$g(t) = \frac{1}{\sqrt{(2\pi)}\,\sigma(\lambda)}\,e^{-(t-t_0)^2/2\sigma(\lambda)^2}, \tag{5}$$

that is

$$I_1(t) = f_1(t) * g(t)$$
$$= \frac{1}{2\alpha}\,e^{-\sigma^2/2\alpha^2}\cdot e^{-\sqrt{2}(\sigma/\alpha)u}[1+\mathrm{Erf}(u)], \tag{6}$$

where

$$u \equiv \frac{1}{\sqrt{2}}\left(\frac{t-t_0}{\sigma} - \frac{\sigma}{\alpha}\right),$$

and

$$\mathrm{Erf}(u) \equiv \frac{2}{\sqrt{\pi}}\int_0^u e^{-y^2}\,dy.$$

In a similar way but starting with eq. (3) we arrive at

the second function

$$I_2(t) = \frac{1}{\sqrt{\pi}} \cdot \frac{\sigma^2}{a^3} \cdot e^{-\alpha^2/2a^2} \cdot e^{-\sqrt{2}(\sigma/a)u} \times \left\{ \frac{\sqrt{\pi}}{4} [1 + \mathrm{Erf}(u)] \cdot (1 + 2u^2) + \tfrac{1}{2} u\, e^{-u^2} \right\}, \quad (7)$$

where

$$u = \frac{1}{\sqrt{2}} \left(\frac{t - t_0}{\sigma} - \frac{\sigma}{a} \right).$$

Eqs. (2)–(7) are normalised to unit area.

Thus, the three parameters t_0, σ and α (or t_0, σ and a) characterize the shape and position of a single peak, and an additional scale factor A gives its integrated intensity.

Our formulae (6) and (7) indicate that the peak leading edge (on the short TOF side) has basically a Gaussian behaviour, while the trailing edge is controlled by the source exponential decay.

It is worth emphasizing that the direct association of geometric uncertainties with a Gaussian distribution and the neutron source emission with the distribution defined by eq. (2) [or eq. (3)] represents an oversimplification of the actual situation. Indeed, any symmetrical effect will contribute to the parameter σ (as does the electron time distribution in each LINAC pulse), whereas nonsymmetrical effects will affect α or a (like the spatial uncertainty of the detection point inside the ^{3}He tube). This topic is further discussed in section 4.

The solid angle covered by our detectors is small, and it is therefore possible to choose a mean value of $\sin\theta$ to relate Q and λ. The use of eq. (6) or (7) as they are, without any integration over the λ window, is a very good approximation in the present case. The extension to wider solid angles is discussed later.

Individual least-squares fits to eighteen isolated peaks starting with the (211) and ending with the (732) can readily be performed on the measured Mo spectrum since the base-line can easily be subtracted. In all cases the least squares function is smaller with eq. (6) than with eq. (7), but the difference is small. In fig. 2 the two curves are shown together with the experimental points for the peak (321). Both fits are indeed indistinguishable in the linear scale of fig. 3, where the broken lines represent the emission-time distributions for the two models.

For all the wavelengths considered the Cd sheet in the sandwich moderator is a black shielding, therefore the time distribution of the emission of neutrons with a given λ is only controlled by the 6 mm thick moderator disk. A short 2 h run was done subsequently with the same sample, but with the Cd sheet removed from the source, thus leaving the full 25 mm thick moderator. It

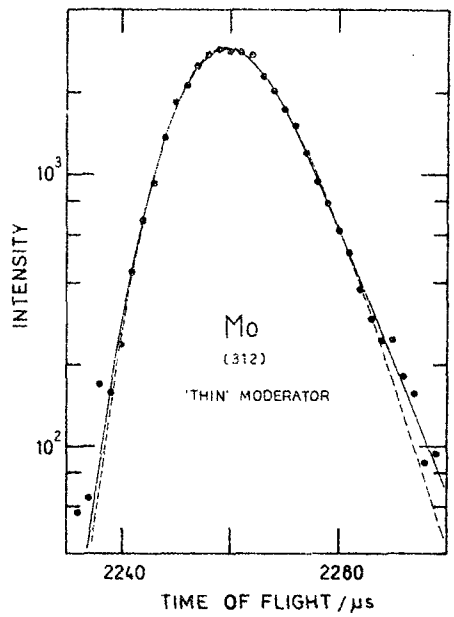

Fig. 2. The (312) peak of Mo. The closed circles show the observed intensity when the 6 mm thick moderator was used. The full line shows the computed profile from eq. (6), whereas the dotted line is that from eq. (7).

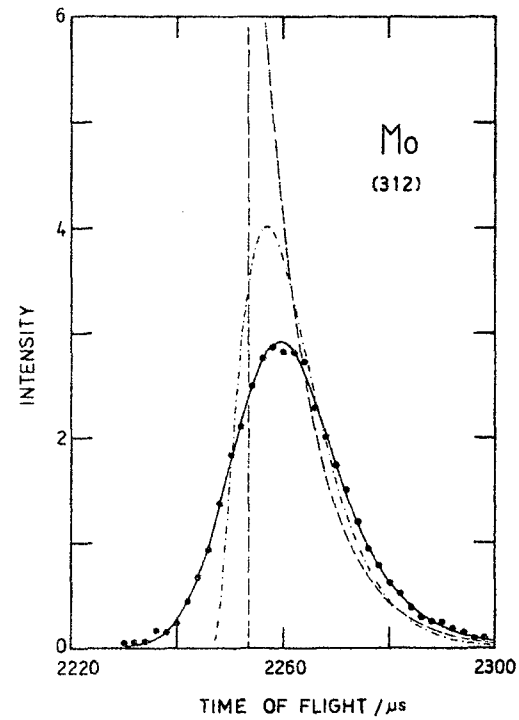

Fig. 3. The (312) peak of Mo. The closed circles show the experimental data and the full line is the fitted lineshape. The broken-line curves correspond to the two models used to describe the source emission-time distribution.

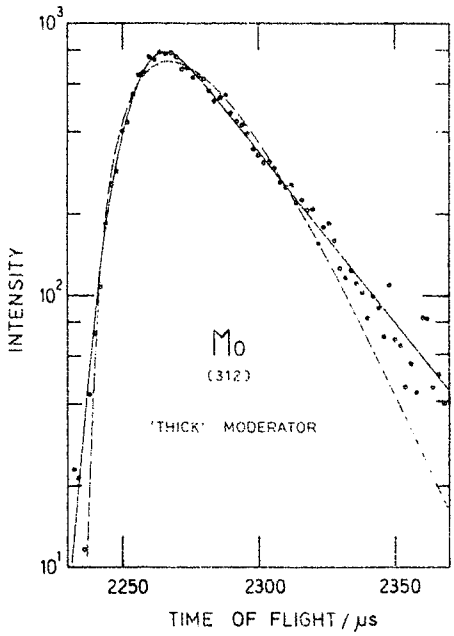

Fig. 4. Same notation as in fig. 2, but with the 25 mm thick neutron source.

was expected that the thicker source would show more significant discrepancies between both models. This did happen, but the best fit again favoured the simple exponential model against the infinite moderator model. Fig. 4 shows this fact for the same (321) peak.

4. Variation of the parameters

As stated before, the usefulness of the knowledge of the peak shapes lies in the possibility of extrapolation towards the high Q region. In order to do that, the observed variations of the parameters should be correlated to the physical reasons that induce such variations along the TOF scale.

4.1. Variation of t_0

Eq. (1) gives $t = c/Q$, and taking into account the effect of an electronic delay:

$$t_0 = c/Q + t_0'. \tag{8}$$

Fig. 5 shows this dependence for the measured peaks, where t_0 is the best fit and Q is determined from Bragg's law, the Miller indices and the cell parameter [7].

We obtained the values

$c = (16724.0 \pm 3.5)\ \mu s/Å$,

$t_0' = (14.8 \pm 0.4)\ \mu s$,

for the present experiment.

4.2. Geometric effects

Let us consider the uncertainties in the spatial coordinates of the three events: emission, scattering and detection. The axial symmetry inherent in the powder sample experiment and the relatively small values of the peak widths allow the problem to be linearized in terms of the angle θ and the length l, that is, to consider the effect as caused by two independent errors in θ and l. We will consider a single detector in this analysis: the addition of more detectors should not significantly modify the peak broadening in a time focussed configuration.

4.2.1. Influence of $\Delta\theta$

Let $\Delta\theta$ be the total angular uncertainty in the scattering process which is due to the finite dimensions of the emitting surface and detector. The different moving Debye–Scherrer cones * do cross the fixed detector one after the other, each having the same angular broadening when crossing. Both the time width of the peak and its integrated intensity are proportional to the time of overlap of cone and detector, and this time is inversely proportional to the sweeping "angular velocity" $d\theta/dt$. From the Bragg condition and the expression of the wavelength λ in terms of the neutron TOF over a distance l, the velocity is calculated to be

$$\frac{d\theta}{dt} = \left(\frac{h}{m_n l}\right)\frac{\operatorname{tg}\theta}{\lambda},$$

and therefore

$$\Delta t|_{\Delta\theta} = \frac{\Delta\theta}{(d\theta/dt)} = \left(\frac{m_n l}{h}\right)\frac{\Delta\theta}{\operatorname{tg}\theta}\lambda.$$

The same kind of dependence on λ holds for the integrated intensity, and this is the ultimate reason for the extra λ factor multiplying the cross section in a TOF peak intensity calculation.

4.2.2. Influence of Δl

The experimental arrangement in our case was such that most of the error in the path length determination results from the uncertainty in the scattering place inside the sample.

* In a steady state powder diffraction experiment, Bragg's law dictates that particles of a given wavelength are scattered into cones, each one corresponding to reciprocal lattice vectors of modulus τ. This concept loses much of its meaning in neutron TOF diffraction experiments, as neutrons of different wavelengths are scattered by the same family of planes τ into surfaces which evolve in time according to the equation

$t\tau = (4\pi m_n/h) l \sin\theta$.

However, we can reconcile this picture with that of Debye–Scherrer cones if we think of them as moving cones.

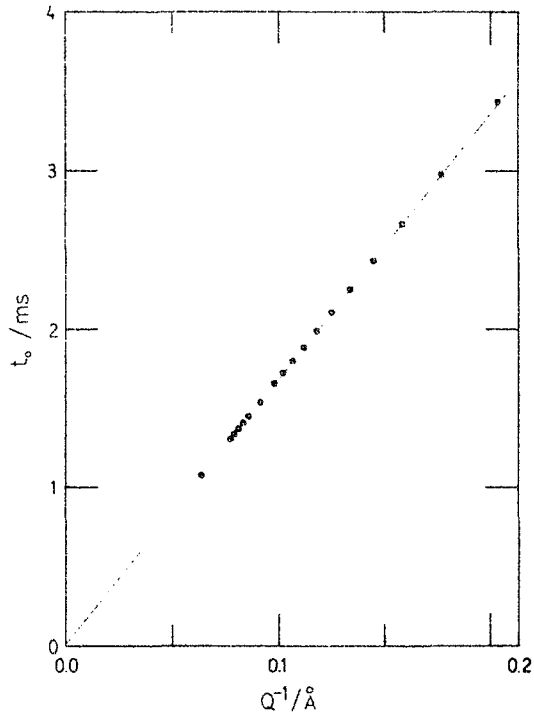

Fig. 5. Variation of the parameter t_0 of eq. (6) with the inverse of scattering vector Q.

If the neutron beam is not severely attenuated in the sample then all volume elements are likely to produce the same number of scattered neutrons. The uncertainty in time will be inversely proportional to the neutron velocity, and therefore

$$\Delta t|_{\Delta t\text{sample}} \sim \lambda .$$

To be consistent with the one-collision model, which is favoured in the shape analysis of individual peaks, we should also assume that the probability of emission is a constant as a function of depth inside the 6 mm thick moderator. Again

$$\Delta t|_{\Delta t\text{ source}} \sim \lambda .$$

The equivalent effect in the detector is not symmetric. The distribution in time of the detected neutrons is an exponential independent of λ as long as the absorption cross section of ^{3}He behaves as $1/v$. The exponential is cut down at the detector edge, that is at a time L/v, where L is the detector thickness. The mean detection time

$$\bar{t}_{\text{det}} \equiv \frac{\int_0^{L/v} t\, e^{-nx\sigma}\, dt}{\int_0^{L/v} e^{-nx\sigma}\, dt} = \frac{1}{cn} - \frac{L}{v}\frac{1}{e^{cnL/v}-1},$$

(where $x = vt$; $\sigma = c/v$), will be proportional to λ for small efficiencies (short wavelengths) and constant for high efficiencies (long wavelengths).

A rough calculation performed by convoluting this asymmetrical time effect with the emission-time effect shows that the measurable slope of the trailing edge will only be that of the moderator emission-time. The contribution of this effect (considered as symmetric) to the Gaussian amounts to only about 10% of the measured σ value, and any deviation from the $\Delta t \sim \lambda$ will hardly be detected.

A similar asymmetrical time effect would be produced by a strong absorbing sample and the discussion would then follow the same line as that for the detection time.

We can therefore expect that the combined effect of geometric uncertainties will produce a Gaussian width proportional to the neutron wavelength

$$\sigma(\lambda) = \sigma_0 + b\lambda , \tag{9}$$

where the constant has been added to account for additional small effects such as the width of the electron LINAC pulse. Fig. 6 shows $\sigma(\lambda)$ derived from the peaks under consideration, clearly supporting the parameterization of eq. (9).

We obtained for our experiment the values

$$\sigma_0 = (0.18 \pm 0.25)\ \mu s,$$

$$b = (4.55 \pm 0.15)\ \mu s/\text{Å}.$$

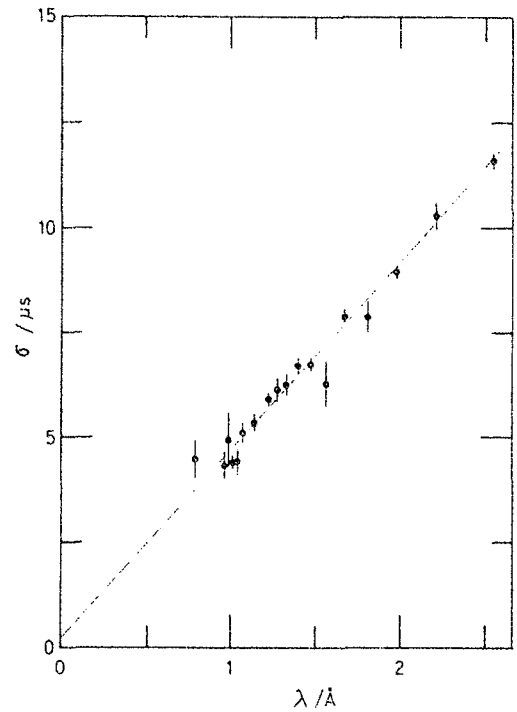

Fig. 6. Variation of the lineshape parameter σ with neutron wavelength.

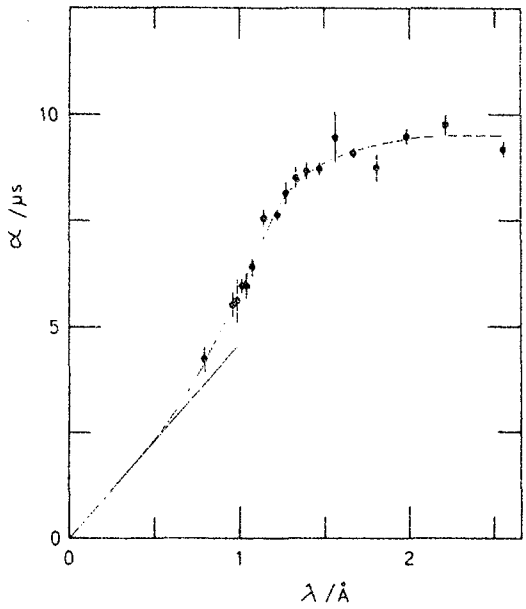

Fig. 7. Variation of the lineshape parameter α with neutron wavelength. The full line below 1 Å is the calculated mean emission time from slowing down theory for our polypropylene moderator.

4.2.3. Variation of α

The one-collison model included in eq. (6) was favoured by the shape anlysis as stated before. The least squares fit performed using this model yielded one α value for each peak. The results are shown in fig. 7. The straight $1/v$ line below 1 Å corresponds to the mean emission-time calculated for our moderator material using slowing down theory [8]:

$$\alpha[\mu s] = 4.51\,\lambda[\text{Å}]$$

According to the experimental results a constant limit is reached at long wavelengths showing a thermalization-like behaviour. However, this should not be due to the attainment of an equilibrium situation but caused by neutron leakage in our large buckling moderator.

5. Discussion

The description of the Bragg peak shape through an analytical function dependent on few parameters simplifies the analysis of a TOF scattering spectrum.

The elastic Q scale can be completely known in terms of the measured time channel number by using a polycrystalline sample as a calibration standard. The cell parameter of a standard could probably be known with five significant digits, much more accuracy than that given by the measurements of flight distances and scattering angles.

Each different set of planes gives an input function to the spectrometer which can be considered a δ-function in Q. The resolution function, which is the response of the spectrometer to such input, is the observed Bragg peak. In general

$$\psi_{\text{meas}}(t) = \text{Resolution} * \psi_{\text{real}} = \int_{-\infty}^{+\infty} R(t-t')\psi_{\text{real}}(t')\,\mathrm{d}t'.$$

The exact dependence of Q on t as given by eq. (1) is replaced in the calibration procedure by an empirical relation $Q(t'')$ obtained by arbitrarily assigning a zero to the t axis of the response function. The deconvolution of the calibration spectrum gives a set of δ's situated at points t'' which are dependent on the choice of the zeros and are the calibration points for $Q(t'')$. Useful points to take as zeros are:

1) t_0 in our model of eq. (6),
2) the maximum of the peak,
3) its centre of mass.

Once an expression is found and a zero is chosen for $R(t)$, any measured spectrum can be deconvoluted to obtain the true one. The true spectrum obtained in this way is of course independent of the particular calibration $Q(t'')$.

If only a first approximation is to be used in the deconvolution process, namely to suppose R to be a δ-function, then it is convenient to choose the centre of mass of the calibration peak as the zero for $R(t)$. In this case the measured spectrum can be taken as the real one. A procedure like this will usually give satisfactory results in those cases where the TOF diffraction pattern consists of a slowly varying function (i.e. liquid or amorphous samples) and all that is required is a proper calibration of the elastic Q scale.

Any mathematical description of the diffraction lineshape should be equally valid as far as the extraction of the true spectrum is concerned (in the elastic Q scale). Nevertheless, it is always useful to extract information from outside the range in which the equation can be tested. The extrapolation towards higher Q is more reliable if the description is based on physical grounds, as our eq. (6), which proved to reproduce satisfactorily the Bragg peaks for both the thick and thin moderators. In practice, we did obtain t_0 and σ from the four parameter least squares fit performed on the 18 considered peaks, and afterwards, by virtue of their well defined wavelength dependence, we performed a second minimization considering only the non-linear α and A parameters as variables. The errors assigned to the quoted α values could be slightly underestimated.

In order to increase the counting rate without significantly changing the resolution, the solid angle can be increased by adding more detectors situated on the Qt = const. surface. The peak shape could then be

calculated by integration of eq. (6) over the solid angle, or more precisely over the corresponding range of neutron wavelengths, and weighted with the λ-dependent cross section, incident spectrum and detector efficiency.

References

[1] C.G. Windsor and R.N. Sinclair, Acta Cryst. A 32 (1976) 395.

[2] D.H. Day and R.N. Sinclair, Nucl. Instr. and Meth. 72 (1969) 237.

[3] J.M. Carpenter et al., Proc. Neutron Diffraction Conf. Petten (1975) p. 192.

[4] I. Cole and C.G. Windsor, Nucl. Instr. and Method. 171 (1980) 107.

[5] K.F. Graham and J.M. Carpenter, Nucl. Instr. and Meth. 85 (1970) 163.

[6] In a recent work [J. Appl. Cryst. 12 (1979) 365] Suortti et al. have shown that the observed profile of a powder reflection in a monochromatic beam experiment is better described by a Voigt function. The difference from a Gaussian is small enough to be neglected in the present work.

[7] a(Mo) = 3.1469 Å, from C.H. MacGillavry and G.D. Rieck, International tables for X-ray crystallography (Kynoch Press, 1968) vol. 3.

[8] K.H. Beckurts and K. Wirtz, Neutron physics (Springer Verlag, 1964) p. 168.